

Dynamics of electron attachment and photodissociation in iodide-uracil-water clusters via time-resolved photoelectron imaging

Alice Kunin, Wei-Li Li, and Daniel M. Neumark

Citation: *The Journal of Chemical Physics* **149**, 084301 (2018); doi: 10.1063/1.5040673

View online: <https://doi.org/10.1063/1.5040673>

View Table of Contents: <http://aip.scitation.org/toc/jcp/149/8>

Published by the [American Institute of Physics](#)

Articles you may be interested in

[Communication: A mean field platform for excited state quantum chemistry](#)

The Journal of Chemical Physics **149**, 081101 (2018); 10.1063/1.5045056

[Using an iterative eigensolver and intertwined rank reduction to compute vibrational spectra of molecules with more than a dozen atoms: Uracil and naphthalene](#)

The Journal of Chemical Physics **149**, 064108 (2018); 10.1063/1.5039147

[Lipids with bulky head groups generate large membrane curvatures by small compositional asymmetries](#)

The Journal of Chemical Physics **149**, 084901 (2018); 10.1063/1.5038427

[The ring-opening channel and the influence of Rydberg states on the excited state dynamics of furan and its derivatives](#)

The Journal of Chemical Physics **149**, 084303 (2018); 10.1063/1.5024655

[Characterization of the vibrational properties of copper difluoride anion and neutral ground states via direct and indirect photodetachment spectroscopy](#)

The Journal of Chemical Physics **149**, 084302 (2018); 10.1063/1.5040122

[Bond selective dissociation of methane \(CH₃D\) on the steps and terraces of Pt\(211\)](#)

The Journal of Chemical Physics **149**, 074701 (2018); 10.1063/1.5041349

PHYSICS TODAY

WHITEPAPERS

ADVANCED LIGHT CURE ADHESIVES

Take a closer look at what these environmentally friendly adhesive systems can do

READ NOW

PRESENTED BY
 **MASTERBOND**
ADHESIVES | SEALANTS | COATINGS

Dynamics of electron attachment and photodissociation in iodide-uracil-water clusters via time-resolved photoelectron imaging

Alice Kunin,¹ Wei-Li Li,^{1,a)} and Daniel M. Neumark^{1,2,b)}

¹Department of Chemistry, University of California, Berkeley, California 94720, USA

²Chemical Sciences Division, Lawrence Berkeley National Laboratory, Berkeley, California 94720, USA

(Received 19 May 2018; accepted 4 August 2018; published online 22 August 2018)

The dynamics of low energy electron attachment to monohydrated uracil are investigated using time-resolved photoelectron imaging to excite and probe iodide-uracil-water ($I^- \cdot U \cdot H_2O$) clusters. Upon photoexcitation of $I^- \cdot U \cdot H_2O$ at 4.38 eV, near the measured cluster vertical detachment energy of $4.40 \text{ eV} \pm 0.05 \text{ eV}$, formation of both the dipole bound (DB) anion and valence bound (VB) anion of $I^- \cdot U \cdot H_2O$ is observed and characterized using a probe photon energy of 1.58 eV. The measured binding energies for both anions are larger than those of the non-hydrated iodide-uracil ($I^- \cdot U$) counterparts, indicating that the presence of water stabilizes the transient negative ions. The VB anion exhibits a somewhat delayed 400 fs rise when compared to $I^- \cdot U$, suggesting that partial conversion of the DB anion to form the VB anion at early times is promoted by the water molecule. At a higher probe photon energy, 3.14 eV, I^- re-formation is measured to be the major photodissociation channel. This product exhibits a bi-exponential rise; it is likely that the fast component arises from DB anion decay by internal conversion to the anion ground state followed by dissociation to I^- , and the slow component arises from internal conversion of the VB anion. *Published by AIP Publishing.*
<https://doi.org/10.1063/1.5040673>

I. INTRODUCTION

Low energy electrons have been shown to induce single and double strand breaks in DNA and can ultimately contribute to mutations, genetic damage, and cancer.¹ Electronic structure calculations indicate that the nucleobase may be the site of initial electron attachment for DNA²⁻⁴ and that electron attachment can form either a conventional valence bound (VB) anion by attachment to the π^* orbital of the base^{3,5} or a dipole bound (DB) anion due to the large molecular dipole moments of nucleobases.⁶ Dissociative electron attachment experiments suggest that an initially formed DB state acts as a gateway to the formation of a VB anion.⁷ Formation of these transient negative ions (TNIs) then leads to the fragmentation of gas phase nucleobases, nucleosides, and nucleotides.^{8,9} Our group has previously examined the dynamics of low energy electron attachment to the nucleobases uracil, thymine, and adenine via time-resolved photoelectron imaging (TRPEI) of iodide-nucleobase clusters.¹⁰⁻¹² We observed the formation and decay of DB and VB TNIs along with photofragmentation to form I^- .¹³ The addition of water has been shown to increase the electron affinity of nucleobases,¹⁴ mediate nucleobase proton transfer,¹⁵ and affect the excited state lifetimes and ultimately the photostability of pyrimidine nucleobases, specifically thymine.^{16,17}

In this study, we examine the dynamics of electron attachment to monohydrated uracil and the subsequent dissociation channels using TRPEI of iodide-uracil-water ($I^- \cdot U \cdot H_2O$) clusters and compare these results to non-hydrated iodide-uracil ($I^- \cdot U$) in order to assess the role of microhydration in these dynamics.

Photoelectron spectroscopy is a powerful tool to detect and identify the presence of both DB and VB anions as they are readily distinguished by differing electron binding energies (eBEs) as well as photodetachment spectral profiles.^{18,19} The excess electron of the DB anion is bound by the molecular dipole moment. Hence, the electron binding energy is very low, often less than 100 meV, and the photoelectron spectrum comprises a narrow peak since the geometry of the weakly bound diffuse anion does not differ significantly from that of the neutral. In VB anions, on the other hand, the excess electron occupies a valence orbital. Even when the neutral species on which the VB anion is based has a closed shell, these anions exhibit higher binding energies of hundreds of meV and more significant geometric distortion from the structure of the corresponding neutral, yielding broad photoelectron spectral profiles. In the case of both uracil and uracil-water, the VB anion geometric distortion is largely in the ring puckering coordinate.^{10,20}

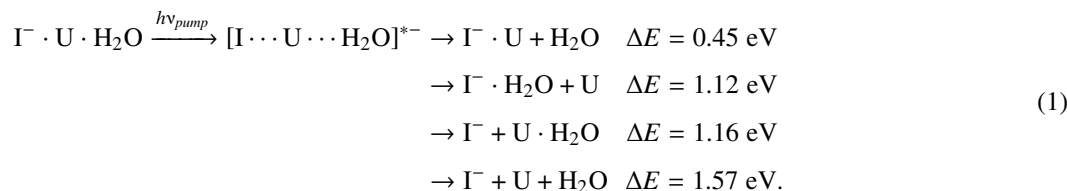
Uracil-water anion clusters have been previously studied with photoelectron spectroscopy by Bowen, Weinkauff, and co-workers.^{14,21} Although the ground state of the gas phase uracil anion is a DB state,^{18,22} only a VB state is evidenced in the photoelectron spectrum of $U^- \cdot H_2O$. The $U^- \cdot H_2O$ VB anion was measured to have a vertical detachment energy (VDE), the

^{a)}Current address: Lam Research Corporation, 4650 Cushing Pkwy., Fremont, California 94538, USA.

^{b)}Author to whom correspondence should be addressed: dneumark@berkeley.edu.

energy difference between the anion and the neutral species at the equilibrium geometry of the anion, of approximately 850 meV. Theory has suggested for both uracil-water^{23,24} and thymine-water anion clusters²⁵ that the VB anion is preferentially stabilized over the DB anion as a result of the interaction energy of the solvating species being greater for the higher density excess electron distribution in the VB anion than in the DB anion.

In the present study, we examine the dynamics of TNI formation and decay for $\text{I}^- \cdot \text{U} \cdot \text{H}_2\text{O}$ clusters photoexcited near the cluster VDE using TRPEI. Photoexcitation with an ultraviolet photon initiates electron transfer from the iodide to the nucleobase moiety. Photoexcitation in this energy regime is expected to form either or both the DB and the VB anions, and these nascent TNIs may energetically access several possible decay channels, calculated in this work,²⁶ including



The TNIs can also undergo autodetachment to one or more neutral species plus an electron.

We employ two different probe photon energies to photodetach the TNIs and ionic photodissociation products to examine the dynamics for the formation and decay of each species. A probe pulse of 1.58 eV is able to photodetach the relatively weakly bound DB and VB anions, as both TNIs generally have electron binding energies below 1 eV. A higher energy probe pulse of 3.14 eV is also used here to detach ionic photofragments, all of which have significantly higher binding energies; the electron affinity of atomic iodine is 3.059 eV, for example.²⁷

Here, we observe the formation of both DB and VB anions from photoexcited $\text{I}^- \cdot \text{U} \cdot \text{H}_2\text{O}$. Both TNIs exhibit a larger binding energy than the DB and VB anions from the analogous process in $\text{I}^- \cdot \text{U}$, indicating stabilization of the anions by the interaction of water. Following photoexcitation, the $\text{I}^- \cdot \text{U} \cdot \text{H}_2\text{O}$ DB anion is observed instantaneously while the VB anion signal exhibits a rise time of ~ 400 fs suggesting that the DB anion undergoes a partial conversion to form the VB anion. A similar delay was seen for $\text{I}^- \cdot \text{U}$ complexes excited near their VDE, but the distinction between DB and VB formation dynamics is more pronounced here. The I^- photofragment signal exhibits a bi-exponential rise of ~ 7 ps and ~ 320 ps, likely arising from TNI decay at early times by internal conversion (IC) to the anion ground state by back-electron transfer to the I atom, followed by the loss of I^- . It is possible that the faster I^- rise originates from the DB anion and the slower rise originates from the VB anion.

II. EXPERIMENTAL AND THEORETICAL METHODS

The TRPEI apparatus has been described in detail previously^{28,29} and is briefly summarized here. $\text{I}^- \cdot \text{U} \cdot \text{H}_2\text{O}$ clusters were formed by passing approximately 550 kPa helium carrier gas over a reservoir of iodomethane and a second reservoir of deionized liquid water. Both reservoirs and the connecting gas line were heated to approximately 40 °C with heating

tape. The gas was passed through a pulsed Even-Lavie valve operating at 500 Hz that contained a cartridge of solid uracil (Sigma-Aldrich, $\geq 99.0\%$) heated to 220 °C. The gas mixture was supersonically expanded into vacuum through a ring electrode ionizer. The resultant anionic clusters were perpendicularly extracted using a Wiley McLaren time-of-flight mass spectrometer³⁰ and mass-selected to isolate the $\text{I}^- \cdot \text{U} \cdot \text{H}_2\text{O}$ species.

The $\text{I}^- \cdot \text{U} \cdot \text{H}_2\text{O}$ clusters were excited and photodetached by femtosecond pump and probe laser pulses delayed by a delay stage. Two pump-probe schemes were used in this study: the pump pulse of 283 nm (4.38 eV) was used with either an infrared probe pulse of 785 nm (1.58 eV) or an ultraviolet probe pulse of 395 nm (3.14 eV). A KMLabs Griffin oscillator and Dragon amplifier were used to generate 40 fs laser pulses centered at 785 nm with 1.85 mJ/pulse at a repetition rate of 1 kHz. These pulses were split to an optical parametric amplifier (LightCon TOPAS-C) to generate the pump pulses and to a frequency-doubling setup using a β -barium borate (BBO) crystal to generate the probe pulses. The pump and frequency-doubled probe pulse energies were 12 μJ /pulse at 283 nm and 65 μJ /pulse at 395 nm, respectively. Alternatively, the residual fundamental was recovered from the doubling process and used as a probe with energies of 80 μJ /pulse at 785 nm. The cross-correlation of the pump and probe laser pulses was approximately 185 fs for 283 nm/785 nm and 220 fs for 283 nm/395 nm.

The resultant photoelectrons were analyzed by velocity map imaging³¹ on a position-sensitive chevron-stacked microchannel plate detector coupled to a phosphor screen and imaged by a charge-coupled device camera. Basis-set expansion (BASEX) methods³² were used to reconstruct the photoelectron kinetic energy (eKE) distributions.

Several of the lowest-lying possible conformations of the $\text{I}^- \cdot \text{U} \cdot \text{H}_2\text{O}$ cluster were calculated here to better understand the geometry and energetics of the experimentally observed $\text{I}^- \cdot \text{U} \cdot \text{H}_2\text{O}$ clusters. The Gaussian 09 computing package³³ was used to calculate the optimized geometries and energies of

the $\text{I}^- \cdot \text{U} \cdot \text{H}_2\text{O}$ cluster at the MP2 level with an augmented Dunning basis set aug-cc-pVDZ for C, H, O, and N atoms and an expanded basis set with an increased set of diffuse functions aug-cc-pVDZ(-pp) for iodide.³⁴ Following geometry optimization, the vibrational frequencies for each of the cluster structures were calculated to confirm that each structure is a true minimum on the potential energy surface. For each of these anionic conformers, the corresponding structures and dipole moments for neutral iodine-uracil-water were also calculated both in the anion ground state geometry (single point calculation) and in the optimized neutral geometry, as well as the optimized geometry for neutral uracil-water, without iodine. This was done to estimate structural changes and binding properties of the $\text{I}^- \cdot \text{U} \cdot \text{H}_2\text{O}$ DB anion, as described in more detail in Sec. V A. For the lowest-lying anion conformer of $\text{I}^- \cdot \text{U} \cdot \text{H}_2\text{O}$ calculated here, we performed equation of motion coupled cluster singles and doubles (EOM-CCSD) excited state calculations [EOM-CCSD/aug-cc-pVDZ(-pp)] to examine the nature of the possible electronic transitions resulting from photoexcitation.

III. RESULTS

Figure 1 shows a single-photon photoelectron spectrum of $\text{I}^- \cdot \text{U} \cdot \text{H}_2\text{O}$ collected at $h\nu_{\text{photon}} = 4.74$ eV and plotted as a function of electron binding energy (eBE), where $\text{eBE} = h\nu_{\text{photon}} - \text{eKE}$. The peak of this spectrum arises from the direct photodetachment of $\text{I}^- \cdot \text{U} \cdot \text{H}_2\text{O}$ and yields a cluster VDE of 4.40 ± 0.05 eV. This VDE corresponds to photodetachment to the lower iodine spin-orbit state ($^2\text{P}_{3/2}$) from the $\text{I}^- \cdot \text{U} \cdot \text{H}_2\text{O}$ anion. The upper $^2\text{P}_{1/2}$ spin-orbit state is expected to lie approximately 0.94 eV higher in energy^{12,35–37} and is thus energetically inaccessible in this work. The smaller peak near the maximum eBE of 4.74 eV (i.e., the photon energy) is from electrons with $\text{eKE} \cong 0$ eV resulting from autodetachment from photoexcited $\text{I}^- \cdot \text{U} \cdot \text{H}_2\text{O}$; these autodetachment signals have been measured in our previous work on $\text{I}^- \cdot \text{U}$ clusters,^{36,37} among others.

Time-resolved photoelectron spectra of $\text{I}^- \cdot \text{U} \cdot \text{H}_2\text{O}$ at 4.38 eV pump excitation energy and 1.58 eV probe energy are shown as a function of eBE ($=h\nu_{\text{probe}} - \text{eKE}$) up to 1 eV eBE and for early times up to 7 ps in Fig. 2. These spectra exhibit

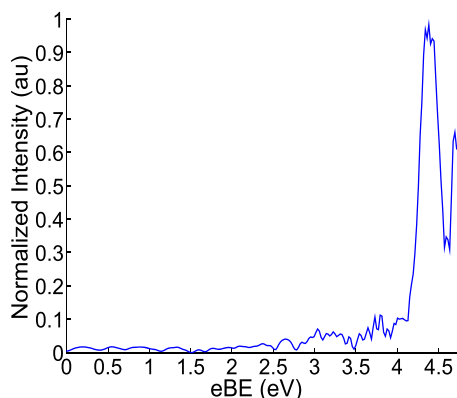


FIG. 1. Single photon, laser noise subtracted, photoelectron spectrum for $\text{I}^- \cdot \text{U} \cdot \text{H}_2\text{O}$ clusters taken at 4.74 eV. The VDE for $\text{I}^- \cdot \text{U} \cdot \text{H}_2\text{O}$ was determined to be 4.40 ± 0.05 eV.

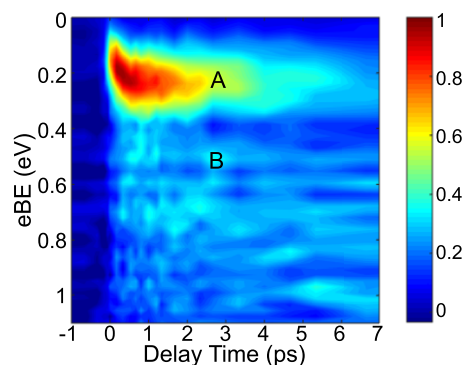


FIG. 2. Representative background-subtracted time-resolved photoelectron spectra for features A (eBE = 0.02–0.38 eV) and B (eBE = 0.40–1.00 eV) at short pump-probe delays for $\text{I}^- \cdot \text{U} \cdot \text{H}_2\text{O}$ at 4.38 eV pump excitation energy and 1.58 eV probe energy.

two features below 1 eV eBE, both of which are prominent at time delays below 5 ps: feature A, a relatively intense and spectrally narrow feature below 0.38 eV eBE, and feature B which is less intense and broader, covering 0.4 eV eBE—1 eV eBE. Based on our previously published results on $\text{I}^- \cdot \text{U}$ clusters at excitation energies near their VDE of 4.11 eV,¹⁰ we can confidently assign feature A as the DB anion of the $\text{I}^- \cdot \text{U} \cdot \text{H}_2\text{O}$ complex and feature B as the VB anion of the $\text{I}^- \cdot \text{U} \cdot \text{H}_2\text{O}$ complex, based on the eBE range and the spectral shape of each feature. As seen prominently in Fig. 2, the eBE of the DB anion shifts to higher binding energy at longer time delays until the feature decays. Figure S1 presents the data of Fig. 2 as a waterfall plot. While feature B may appear to have some structure or progression in the time-resolved photoelectron spectra, the ± 0.05 eV resolution of this experiment precludes the possibility of analyzing these relatively smaller intensity changes.

The time-resolved photoelectron spectra for $\text{I}^- \cdot \text{U} \cdot \text{H}_2\text{O}$ at 4.38 eV pump excitation energy and 3.14 eV probe energy are shown in Fig. 3, plotted from 1.2 to 3.14 eV eBE. The most prominent feature, feature D, is located at 3.06 ± 0.05 eV eBE and is spectrally narrow but very intense, growing in strongly over 10s of ps. Based on its binding energy, spectral shape, and time-dependent monotonic rise, feature D is assigned to the photodetachment of atomic iodide produced

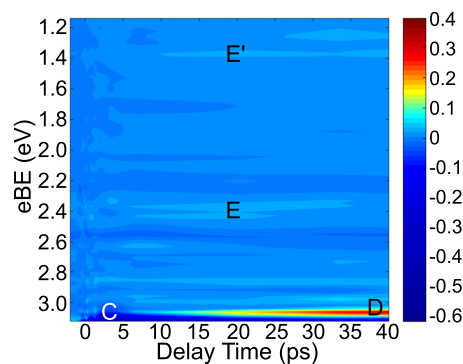


FIG. 3. Representative background-subtracted time-resolved photoelectron spectra for features C (maximum eBE, eKE ~ 0 eV), D (eBE = 3.06 eV), E (eBE = 2.29–2.99 eV), and E' (eBE = 1.14–1.64 eV) for $\text{I}^- \cdot \text{U} \cdot \text{H}_2\text{O}$ at 4.38 eV pump excitation energy and 3.14 eV probe energy.

following the pump photoexcitation of $\text{I}^- \cdot \text{U} \cdot \text{H}_2\text{O}$ clusters. Feature C, located at the maximum eBE edge of the spectrum or approximately 0 eV eKE, is spectrally very narrow and exhibits an initial depletion at early times with intensity recovery at longer times. An analogous feature is also observed at the maximum eBE edge of the TRPEI data at 1.58 eV probe energy but is omitted here from Fig. 2 for clarity as it overlaps with another feature, as described below in more detail. The characteristics of feature C are very similar in nature to those previously observed for autodetachment from $\text{I}^- \cdot \text{U}$ clusters,³⁷ so it can be assigned as autodetachment from photoexcited $\text{I}^- \cdot \text{U} \cdot \text{H}_2\text{O}$ clusters. Figure S2 presents a magnified view of the data in Fig. 3 for the energy region from 3.00 to 3.12 eV to better show the distinction between features C and D.

At lower eBEs, there is a weak intensity broad region exhibiting time dependence from approximately 2.3 eV to 3.0 eV eBE, denoted as feature E, and also from approximately 1.14–1.64 eV eBE, feature E'. Feature E' is also weakly observed in the 1.58 eV probe TRPEI data but overlaps spectrally with the autodetachment feature, and the full feature is not captured by the 1.58 eV probe limit, so it is omitted from Fig. 2 for clarity. Figure S3 presents the data of Fig. 3 as a waterfall plot with feature C omitted to allow a clearer view of features E and E'. Though noisy, these features appear to have

somewhat different rise and decay dynamics from one another. We explore possible assignments for these weak features in the [supplementary material](#).

Multiple low-lying isomers have been calculated for uracil-water^{38–40} and several have been calculated here for $\text{I}^- \cdot \text{U} \cdot \text{H}_2\text{O}$; the resulting structures, relative energies, and VDEs of the lowest-lying six isomers of $\text{I}^- \cdot \text{U} \cdot \text{H}_2\text{O}$ are presented in Table I. Six energetically low-lying unique isomers of $\text{I}^- \cdot \text{U} \cdot \text{H}_2\text{O}$ were found within 2 kcal/mol of one another. It is unsurprising that structures such as those of Table I(a)–I(c) are the lowest lying isomers given that the iodide-water ion-dipole interaction is expected to be stronger than the uracil-water dipole-dipole interaction, but within our heated cluster source, all of these isomers and many more are possible. The calculated VDEs of these clusters are all close to the experimentally measured VDE of 4.40 ± 0.05 eV. The experimental results seen here likely represent an ensemble average of the dynamics of several low-lying isomers.

Table SI presents calculated structures and dipole moments for the neutral iodine-uracil-water in the geometry of both the anion ground state and the optimized neutral, as well as the neutral uracil-water geometry. The anion ground state geometry can be approximated to be the Franck-Condon geometry for the DB anion as it is initially formed, and the

TABLE I. The six energetically lowest-lying calculated structures for $\text{I}^- \cdot \text{U} \cdot \text{H}_2\text{O}$ anion complexes. Relative energies supplied are relative to the ground state structure, 0.00 kcal/mol by definition, and corrected for zero point energies. The (a) and (e) structures are the only ones which have both O–H bonds of water outside of the uracil plane, so the side views for (a) and (e) are provided under their respective structures. The VDEs presented here correspond to the difference in energy between the $\text{I}^- \cdot \text{U} \cdot \text{H}_2\text{O}$ anion and the lower iodine spin orbit state ($^2\text{P}_{3/2}$) of $\text{I} \cdot \text{U} \cdot \text{H}_2\text{O}$ at the equilibrium geometry of the anion.

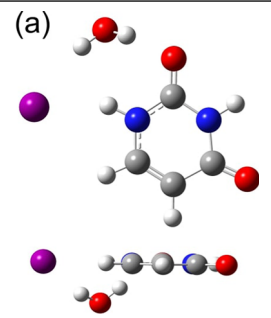
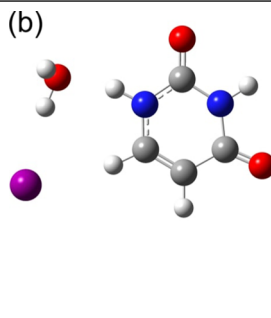
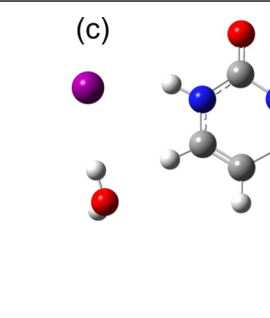
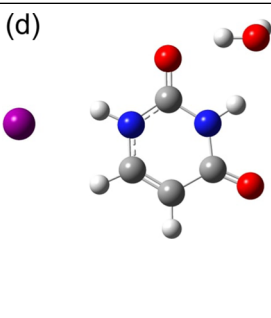
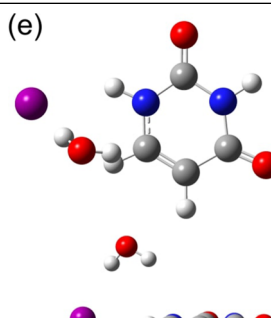
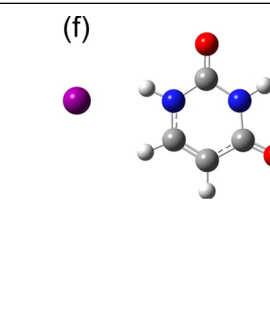
	(a)	(b)	(c)
			
Relative energy (kcal/mol)	0.00	0.59	0.92
VDE (eV)	4.57	4.50	4.62
	(d)	(e)	(f)
			
Relative energy (kcal/mol)	1.65	1.79	1.87
VDE (eV)	4.33	4.62	4.31

TABLE II. EOM-CCSD/aug-cc-pVDZ(-pp) calculated electronic transition channels, energies, and corresponding oscillator strengths for the lowest-lying calculated anion conformer of $\text{I}^- \cdot \text{U} \cdot \text{H}_2\text{O}$, corresponding to the structure in Table I(a). The excitation energies here have not been offset and are the calculated values. See Sec. IV for more details.

Excitation energy (eV)	Oscillator strength	Transition channel	Final state configuration
4.7964	0.0809	$\text{I}(5p)\text{-DB}$	$\text{I}(5p^5)[\text{U} \cdot \text{H}_2\text{O}]^-(\text{DB}^1)$
4.8823	0.1003	$\text{I}(5p)\text{-DB}$	$\text{I}(5p^5)[\text{U} \cdot \text{H}_2\text{O}]^-(\text{DB}^1)$
5.0283	0.1624	$\text{I}(5p)\text{-DB}$	$\text{I}(5p^5)[\text{U} \cdot \text{H}_2\text{O}]^-(\text{DB}^1)$
5.0774	0.0104	$\text{I}(5p)\text{-}\pi^*$	$\text{I}(5p^5)\text{U}^-(\pi^4\pi^*)\text{H}_2\text{O}$
5.0966	0.0282	$\text{I}(5p)\text{-}\pi^*$	$\text{I}(5p^5)\text{U}^-(\pi^4\pi^*)\text{H}_2\text{O}$
5.2240	0.0652	$\text{I}(5p)\text{-}\pi^*$	$\text{I}(5p^5)\text{U}^-(\pi^4\pi^*)\text{H}_2\text{O}$
5.2695	0.1368	$\pi\text{-}\pi^*$	$\text{I}^-(5p^6)\text{U}(\pi^3\pi^*)\text{H}_2\text{O}$

optimized neutral iodine-uracil-water structures serve as an approximation for the equilibrium geometry of the $\text{I}^- \cdot \text{U} \cdot \text{H}_2\text{O}$ DB anion since the diffuse, excess electron is expected to minimally perturb the neutral geometry. These structures can be used to estimate the possible evolution of the geometry of the DB anion as well as the magnitude of the dipole moment binding the excess electron and are discussed in more detail in Sec. V A.

Table II presents the results of the EOM-CCSD excited state calculation for the lowest-lying calculated $\text{I}^- \cdot \text{U} \cdot \text{H}_2\text{O}$ anion conformer, corresponding to the structure in Table I(a). Seven excited state transition channels were calculated to exist below 5.3 eV; the three lowest in energy are within 0.25 eV of one another and correspond to transitions from an iodide $5p$ orbital to the DB orbital with considerable oscillator strength. The calculated DB orbital and the calculated π^* orbital accessed in the higher energy transitions are shown in Fig. S4. In similar calculations performed by our group for $\text{I}^- \cdot \text{U}$,¹³ the calculated energy values were compared to an experimental photodepletion (absorption) spectrum of $\text{I}^- \cdot \text{U}$ and found to exceed the experimental energies by 0.52 eV. No experimental photodepletion spectrum has been measured for $\text{I}^- \cdot \text{U} \cdot \text{H}_2\text{O}$ but this approximate 0.5 eV energy overestimate is expected to be similar for the $\text{I}^- \cdot \text{U} \cdot \text{H}_2\text{O}$ results here, which would place these three lowest transition channels in the range of approximately 4.28 eV–4.51 eV, close to the pump excitation energy of 4.38 eV used here. Hence, at this pump energy, one expects excitation to a DB state of the complex. Based on these results for the $\text{I}^- \cdot \text{U} \cdot \text{H}_2\text{O}$ conformer in Table I(a), we can conclude that the effect of the hydrogen bonding of the water molecule to iodide is to increase both the VDE of the cluster and the excitation energy for the formation of the DB state. Thus, for the conformers of Table I(b), I(c), and I(e), the results for these calculated transition channels will likely be similar. For Table I(d) and I(f), the VDE is calculated to be somewhat lower, and likely the excitation energy for the formation of the DB state will be proportionately somewhat lower as well.

IV. ANALYSIS

Feature A in Fig. 2, corresponding to a DB state, shows a pronounced time-dependent shift in its VDE. To better

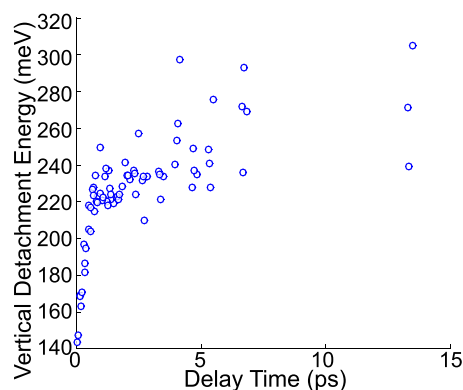


FIG. 4. Concatenated VDEs for feature A for each delay time up to 15 ps. Feature A exhibits a fast increase in VDE from approximately 140 meV to 230 meV within 1 ps followed by a gradual increase in the VDE thereafter until the intensity of the feature decays to a point where it can no longer be fit with an analytical function. After 15 ps, feature A decays to approximately only 20% of its maximum intensity.

quantify this effect, the spectral shape of feature A can be fit to a Gaussian function at all time delays for which the intensity of the feature is non-zero. The binding energy corresponding to the peak of this Gaussian is plotted as a function of pump-probe time delay in Fig. 4. The DB anion VDE shifts from approximately 140 meV to 230 meV in 1 ps and increases to approximately 275 meV in 15 ps. Beyond 15 ps, the intensity of feature A is too small to accurately fit to a Gaussian function.

The normalized, integrated intensities for both the $\text{I}^- \cdot \text{U} \cdot \text{H}_2\text{O}$ DB anion and VB anion (feature B) up to 7 ps time delay are shown together for comparison in Fig. 5. The corresponding intensities out to 300 ps are presented in Fig. 6. To capture the time-dependent dynamics of these features, the integrated signals are fit to the convolutions of a Gaussian instrumental response and multiple exponential functions according to the following equation:

$$I(t) = \frac{1}{\sigma_{cc}\sqrt{2\pi}} \exp\left(\frac{-t^2}{2\sigma_{cc}^2}\right) \cdot \begin{cases} I_0, & t < 0 \\ I_0 + \sum_i A_i \exp\left(\frac{-t}{\tau_i}\right), & t \geq 0 \end{cases} \quad (2)$$

where σ_{cc} is the Gaussian full width at the half-maximum given by the cross-correlation of the pump and probe laser pulses, I_0 is the signal background, A_i are the coefficients of

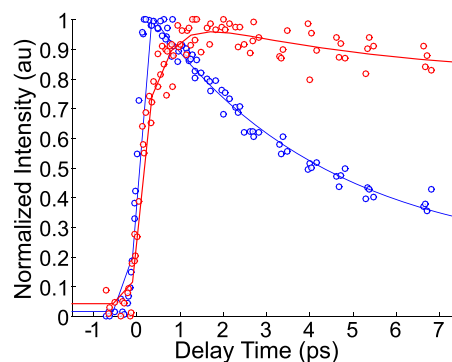


FIG. 5. Concatenated normalized integrated intensities for features A (blue, DB anion) and B (red, VB anion) at short time delays.

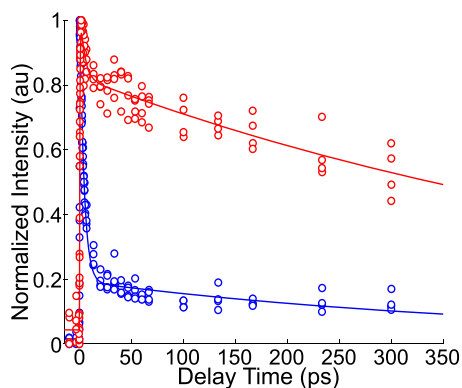


FIG. 6. Concatenated normalized integrated intensities for feature A (blue, DB anion) and feature B (red, VB anion) from excitation at 4.38 eV and probed with 1.58 eV. The rise time for feature A is cross-correlation limited, and the decay is 4.1 ± 0.2 ps and 410 ± 140 ps. The rise time for feature B is 400 ± 140 fs and decays bi-exponentially in 6.1 ± 2.4 ps and 650 ± 100 ps.

the i exponential functions, and τ_i are the corresponding rise or decay lifetimes for each exponential.

Table III summarizes the fit rise and decay time constants for the $\text{I}^- \cdot \text{U} \cdot \text{H}_2\text{O}$ DB and VB anions and for I^- , the exponential fitting function amplitudes A_i , and the intensity ratio of the DB anion to the VB anion. This intensity ratio is measured, as in $\text{I}^- \cdot \text{U}$, for a set time near the intensity maxima of both features, ~ 400 fs, from the un-normalized integrated intensities. Fits to the data in Figs. 5 and 6 based on Eq. (2) are shown as solid blue and red lines for the DB and VB anions, respectively. These fits yield a cross-correlation limited rise time for the DB anion with bi-exponential decay in 4.1 ± 0.2 ps and 410 ± 140 ps and formation of the VB anion in 400 ± 140 fs with bi-exponential decay in 6.1 ± 2.4 ps and

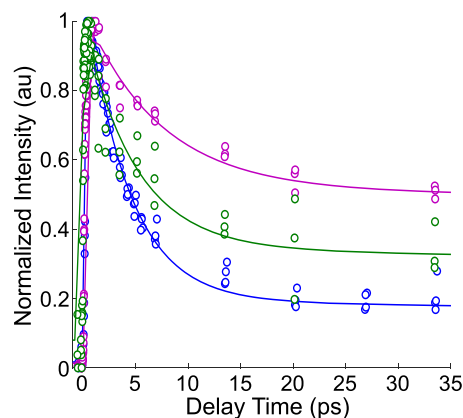


FIG. 7. Comparison of the normalized integrated intensities for the $\text{I}^- \cdot \text{U} \cdot \text{H}_2\text{O}$ DB anion (blue, 20 meV below $\text{I}^- \cdot \text{U} \cdot \text{H}_2\text{O}$ VDE) and the $\text{I}^- \cdot \text{U}$ DB anion (purple, 40 meV below $\text{I}^- \cdot \text{U}$ VDE; green, 30 meV above VDE). The $\text{I}^- \cdot \text{U}$ data are adapted with permission from King *et al.*, J. Chem. Phys. **141**, 224310 (2014). Copyright 2014 AIP Publishing LLC.

650 ± 100 ps. The large error bars for the long-time decays are in part due to the values being longer than the maximum pump-probe delay used in the 1.58 eV probe experiment, 300 ps. For ease of comparison to our previous work on $\text{I}^- \cdot \text{U}$ clusters photoexcited at 40 meV below and 30 meV above the cluster VDE,¹⁰ the fit rise and decay time constants as well as the amplitudes from the exponential fitting functions for $\text{I}^- \cdot \text{U}$ DB and VB anions are also presented in Table III. Additionally, Fig. 7 compares the normalized integrated intensity and exponential fits out to 35 ps for the $\text{I}^- \cdot \text{U} \cdot \text{H}_2\text{O}$ DB anion (blue), to the intensities and fits for the $\text{I}^- \cdot \text{U}$ DB anion photoexcited at VDE -40 meV (purple) and VDE $+30$ meV (green).

TABLE III. Lifetimes and exponential fit coefficients A_i for the DB and VB anions for $\text{I}^- \cdot \text{U} \cdot \text{H}_2\text{O}$ compared to $\text{I}^- \cdot \text{U}$. A_1 refers to the coefficient for τ_{rise} , A_2 for $\tau_{\text{decay},1}$, and A_3 for $\tau_{\text{decay},2}$. The $\text{I}^- \cdot \text{U}$ data for the DB and VB anions are reprinted with permission from King *et al.*, J. Chem. Phys. **141**, 224310 (2014). Copyright 2014 AIP Publishing LLC. The $\text{I}^- \cdot \text{U}$ data for the I^- feature are adapted with permission from Li *et al.*, J. Chem. Phys. **145**, 044319 (2016). Copyright 2016 AIP Publishing LLC.

DB anion								
Cluster	$h\nu_{\text{pump}} - \text{VDE}$ (meV)	τ_{rise} (fs)	$\tau_{\text{decay},1}$ (ps)	$\tau_{\text{decay},2}$ (ps)	A_1	A_2	A_3	DB/VB ratio
$\text{I}^- \cdot \text{U} \cdot \text{H}_2\text{O}$	-20	<185	4.1 ± 0.2	410 ± 140	...	0.88	0.17	1.12
$\text{I}^- \cdot \text{U}$	-40	260 ± 50	7.1 ± 0.7	1200 ± 100	-0.47	0.51	0.50	1.41
$\text{I}^- \cdot \text{U}$	+30	120 ± 90	5.0 ± 0.6	500 ± 130	-0.26	0.66	0.26	1.04
VB anion								
Cluster	$h\nu_{\text{pump}} - \text{VDE}$ (meV)	τ_{rise} (fs)	$\tau_{\text{decay},1}$ (ps)	$\tau_{\text{decay},2}$ (ps)	A_1	A_2	A_3	
$\text{I}^- \cdot \text{U} \cdot \text{H}_2\text{O}$	-20	400 ± 140	6.1 ± 2.4	650 ± 100	-0.60	0.27	0.73	
$\text{I}^- \cdot \text{U}$	-40	200 ± 20	13.9 ± 1.4	450 ± 40	-0.75	0.56	0.44	
$\text{I}^- \cdot \text{U}$	+30	220 ± 40	5.6 ± 1.5	80 ± 30	-0.65	0.54	0.35	
I^-								
Cluster	$h\nu_{\text{pump}} - \text{VDE}$ (meV)	$\tau_{\text{rise},1}$ (ps)	$\tau_{\text{rise},2}$ (ps)	A_1	A_2			
$\text{I}^- \cdot \text{U} \cdot \text{H}_2\text{O}$	-20	6.7 ± 3.8	320 ± 30	-0.15	-0.86			
$\text{I}^- \cdot \text{U}$	-80	17.5 ± 1.6	150 ± 10	-0.16	-0.79			

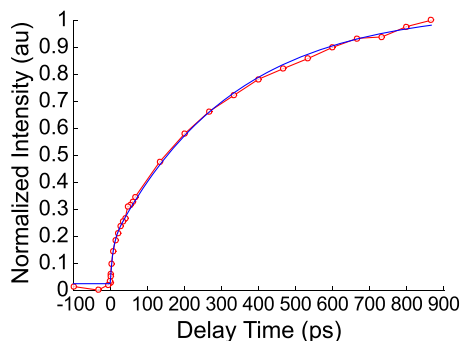


FIG. 8. Normalized integrated intensity for feature D at 4.38 eV pump excitation energy and 3.14 eV probe energy. Feature D rises bi-exponentially with time constants of 6.7 ± 3.8 ps and 320 ± 30 ps.

Figure 8 presents the normalized integrated intensity and fitted bi-exponential rise for the iodide signal produced from the photoexcited $\text{I}^- \cdot \text{U} \cdot \text{H}_2\text{O}$. Photodetachment from I^- appears in 6.7 ± 3.8 ps and 320 ± 30 ps. The result for the formation of iodide from $\text{I}^- \cdot \text{U}$ clusters photoexcited 80 meV below the VDE fit with a bi-exponential rise is also presented in Table III for comparison. These data were originally fit in the work of Li *et al.* by a mono-exponential rise function but has been revised here to fit the data more accurately with a bi-exponential fit. These fits are shown for comparison in Fig. S5 and are discussed in more detail in Sec. V.

The normalized integrated intensities for the weak features E and E', which may correspond to two metastable TNI decay products, are shown in Fig. S6. These features are quite noisy but can be fit to a mono-exponential rise and mono-exponential decay. Feature E has a rise time of 3.5 ± 1.4 ps and a decay time of 500 ± 80 ps, and feature E' has a rise time of 8.7 ± 3.7 ps and a decay time of 675 ± 120 ps. Further discussion of these two features is restricted to the [supplementary material](#).

V. DISCUSSION

The work presented here examines the ultrafast dynamics of the DB and VB TNIs for $\text{I}^- \cdot \text{U} \cdot \text{H}_2\text{O}$. The DB anion formed by the photoexcitation of $\text{I}^- \cdot \text{U} \cdot \text{H}_2\text{O}$ near the VDE appears within the cross-correlation of the pump and probe laser pulses, followed by the rise of the VB anion in 400 fs. Here, we examine the dynamics of the prompt formation of $\text{I}^- \cdot \text{U} \cdot \text{H}_2\text{O}$ TNIs and the subsequent decay channels, along with possible pathways for the observed re-formation of iodide as a photofragment. We also provide a comparison to the previously observed dynamics for $\text{I}^- \cdot \text{U}$ clusters photoexcited near the VDE to better understand the role of water in the electron attachment and decay processes.

In our past work on $\text{I}^- \cdot \text{U}$ clusters photoexcited near the VDE, the TNI lifetimes and exponential fit coefficients were found to exhibit considerable excitation energy dependence.¹⁰ It is thus central in this discussion for the comparison of $\text{I}^- \cdot \text{U} \cdot \text{H}_2\text{O}$ clusters to $\text{I}^- \cdot \text{U}$ clusters to distinguish between dynamical effects that are due to the addition of water versus those effects that likely stem from differences in pump excitation energy or internal energy. To aid in this comparison,

the previous $\text{I}^- \cdot \text{U}$ DB and VB anion results for pump excitation energies both 40 meV below the VDE (-40 meV) and 30 meV above the VDE ($+30$ meV) are compared here to $\text{I}^- \cdot \text{U} \cdot \text{H}_2\text{O}$ clusters photoexcited 20 meV below the VDE (-20 meV). A higher probe energy of 3.61 eV capable of photodetaching I^- was applied only to $\text{I}^- \cdot \text{U}$ clusters photoexcited 80 meV below the VDE.¹³ The iodide re-formation dynamics observed in that work are reconsidered here in light of the present $\text{I}^- \cdot \text{U} \cdot \text{H}_2\text{O}$ results.

We begin by briefly considering the nature of the excited states of the photoexcited $\text{I}^- \cdot \text{U} \cdot \text{H}_2\text{O}$ complex. The EOM-CCSD calculations performed here (Table II), although energetically offset from our experimental results, suggest that the lowest energy transitions activated near the VDE correspond to an electronic transition from the $\text{I}(5p)$ orbital to the DB state of $\text{I}^- \cdot \text{U} \cdot \text{H}_2\text{O}$. These calculated results are similar to the calculations performed previously by our group for the excited state transition channels of $\text{I}^- \cdot \text{U}$,¹³ which also found that the only electronic transitions energetically near the VDE of the complex were the transitions from $\text{I}(5p)$ to the DB orbital, with comparable oscillator strengths to those given in Table II. Thus, the photoexcitation of $\text{I}^- \cdot \text{U} \cdot \text{H}_2\text{O}$ near its VDE is expected to directly access the DB orbital.

Before examining the TNIs separately, it is useful to note first the observed binding energy ranges for each feature. In previous work on $\text{I}^- \cdot \text{U}$ clusters, the DB anion was observed between 0 and 0.2 eV eBE, and the VB anion was observed in the range from 0.3 to 0.7-0.8 eV eBE.¹⁰ Both of these energy ranges are slightly narrower and approximately 0.2 eV lower in maximum eBE than for the corresponding features in $\text{I}^- \cdot \text{U} \cdot \text{H}_2\text{O}$. The increase in eBE for the $\text{I}^- \cdot \text{U} \cdot \text{H}_2\text{O}$ DB and VB anions relative to that seen in TRPEI of $\text{I}^- \cdot \text{U}$ confirms that the water molecule is associated in both TNIs over the course of our measurements and that it stabilizes both the DB and VB anions.

A. Formation and VDE shifting of the DB anion

The formation of the DB state of $\text{I}^- \cdot \text{U} \cdot \text{H}_2\text{O}$ was found to be instantaneous in this work (<185 fs), while for $\text{I}^- \cdot \text{U}$, at -40 meV, the DB anion rise was 260 ± 50 fs and at $+30$ meV, it was 120 ± 90 fs.¹⁰ The $\text{I}^- \cdot \text{U} \cdot \text{H}_2\text{O}$ DB anion rise thus more closely resembles the dynamics of $+30$ meV photoexcited $\text{I}^- \cdot \text{U}$ rather than -40 meV. This result is perhaps unsurprising considering that an analogous VDE-relative pump excitation energy between $\text{I}^- \cdot \text{U} \cdot \text{H}_2\text{O}$ and $\text{I}^- \cdot \text{U}$ may result in differing amounts of internal energy between the two clusters, given that the addition of water, depending on its geometric positioning, will add several vibrational modes to the cluster. Thus, considering this excitation energy dependence, we expect that the fast rise dynamics here for the $\text{I}^- \cdot \text{U} \cdot \text{H}_2\text{O}$ DB anion are similar to the $\text{I}^- \cdot \text{U}$ DB anion.

As shown in Fig. 4, the $\text{I}^- \cdot \text{U} \cdot \text{H}_2\text{O}$ DB anion exhibits an increase in the VDE at early times from 140 meV to approximately 230 meV within 1 ps, followed by a less steep, continued increase thereafter until the anion decays to $<20\%$ of its maximum intensity, which occurs in approximately 15 ps. This is in contrast to the previously observed VDE shifting of iodine-associated nucleobase cluster DB anions in TRPEI

studies^{10,11} where, in the case of $I^- \cdot U$, the VDE of the DB anion increased from 75 meV to 115 meV in approximately 700 fs. It then declined to a long-time value of 95 meV by 20 ps, the VDE of bare U^- , indicating that the I atom had departed. These $I^- \cdot U$ VDE shifting dynamics were found not to exhibit any excitation energy dependence for pump energies within ± 100 meV of the VDE in the previous work on $I^- \cdot U$ clusters. Due to this lack of excitation energy dependence in the VDE shifting, it is apparent that the differences in DB anion VDE shifting between $I^- \cdot U \cdot H_2O$ and $I^- \cdot U$ are effects induced by the presence of the water molecule. We now examine the early-time and long-time VDE shifting dynamics separately.

In iodine-associated DB anions formed in the Franck-Condon region, the exchange repulsion between the electrons of iodine and the DB electron is expected to destabilize the species due to excluded volume effects.^{41–44} This repulsive interaction drives the DB anion to a lower energy geometry from the vertical excitation region to the DB equilibrium geometry; as this interaction is absent in the neutral, the result is an increase in the VDE at early times. Within 1 ps of the DB state formation, the $I^- \cdot U \cdot H_2O$ DB anion VDE is measured to increase approximately 164% from the initial value. In $I^- \cdot U$, the DB anion of $I^- \cdot U$ exhibited a VDE increase from 75 meV to 115 meV in approximately 700 fs or a 153% increase.¹⁰ From this, it appears that the initial rise of the VDE for the $I^- \cdot U \cdot H_2O$ DB anion follows a similar iodine excluded volume perturbation mechanism as $I^- \cdot U$ at early times and thus that the initial VDE increase in $I^- \cdot U \cdot H_2O$ is likely governed by the motion of iodine relative to the uracil-water moiety.

For $I^- \cdot U \cdot H_2O$, after the initial sharp VDE increase, the DB anion VDE is found to increase by ~ 50 meV until approximately 15 ps when the decay of the DB anion is too substantial to analytically fit the VDE. This increase is opposite to the drop in VDE for the DB state of $I^- \cdot U$, although it occurs on a similar time scale. It is possible that the longer-time VDE shifts in the two systems have a similar origin, namely, the loss of an I atom. For all $I^- \cdot U \cdot H_2O$ isomers presented in Table SI, the calculated dipole moment of the neutral $U \cdot H_2O$ species is significantly larger than that of the iodine-associated $U \cdot H_2O$ species, leading to an increase in the binding energy if neutral iodine shifts away. By contrast, I atom loss from the DB state of $I^- \cdot U$ results in a decreased dipole moment and a decrease in the binding energy.¹⁰ Thus, the loss of neutral iodine from the cluster in ~ 15 ps can account for the observed VDE shifting at intermediate times in both $I^- \cdot U \cdot H_2O$ and $I^- \cdot U$.

B. Formation and energetics of the VB anion

In $I^- \cdot U$, the rise of the VB anion subsequent to photoexcitation near the VDE was found to be ~ 200 fs and was largely independent of photon energy. Therefore, the somewhat longer ~ 400 fs VB anion rise seen for $I^- \cdot U \cdot H_2O$ is attributed to the addition of the water molecule. Given that the initial electronic excitation is to the DB state of $I^- \cdot U \cdot H_2O$, the 400 fs rise time may reflect partial conversion of the DB anion to form the VB anion. This mechanism has been suggested

previously from our work on $I^- \cdot U$ clusters photoexcited near the VDE,¹⁰ but the more obvious distinction between the DB and VB rise times in the presence of water argues more strongly in its favor. Moreover, it is now well established from experiment and theory that the VB state of $U^- \cdot H_2O$ is lower in energy than the DB state.^{14,21,23,24} Here, as in our previous work on $I^- \cdot U$, however, there is unfortunately no direct match of VB anion rise and DB anion decay time scales, as has been observed for $I^- \cdot \text{Adenine}$ and $I^- \cdot \text{CH}_3\text{NO}_2$.^{12,45}

Calculations by Takayanagi *et al.* for the DB and VB anions of $U^- \cdot H_2O$ indicate that for various $U^- \cdot H_2O$ DB anion isomers, the barrier height for a DB to VB anion conversion can vary from 0.43 to 3.00 kcal/mol.²⁴ The authors expect the barrier to isomerization of water to a different binding site around uracil to be approximately 1–5 kcal/mol as well and thus predict water-binding-site-change isomerization pathways to be active among the various conformers of the DB anion to form a DB anion with a lower VB anion conversion barrier.²⁴ Therefore, in $I^- \cdot U \cdot H_2O$, it is possible that a small structural change in the water binding site in the DB anion to lower the energetic conversion barrier will delay the VB anion formation relative to that in $I^- \cdot U$ on the order of ~ 100 fs.

C. Decay channels of the DB and VB anion and the re-formation of iodide

The $I^- \cdot U \cdot H_2O$ DB and VB anions exhibit bi-exponential decay dynamics with fast decay lifetimes of 4 ps and 6 ps, respectively, and longer decay lifetimes of 410 ps and 650 ps, respectively, while the iodide photofragment signal exhibits a bi-exponential rise with time constants of approximately 7 ps and 320 ps. We have previously suggested that for $I^- \cdot U$ DB and VB anion bi-exponential decay, the fast decay may be internal conversion to the anion ground state by back-electron transfer to the I atom which then dissociates after some delay to yield $U + I^-$.¹³ For $I^- \cdot U \cdot H_2O$, the observation that the two fast TNI decays are each slightly faster than the fast I^- rise time lends support to this attribution, but here we also consider our past measurements of the I^- signal from iodide-associated clusters to explain the bi-exponential I^- rise dynamics.

Previously, the I^- signal from $I^- \cdot U$ was fit to a mono-exponential function with a rise time of 86 ps. However, as discussed in Sec. IV, an improved fit results from assuming a bi-exponential rise with time constants of 17.5 ± 1.6 ps and 150 ± 10 ps (Table III). A comparison of the mono-exponential and bi-exponential fits for the rise of I^- from $I^- \cdot U$ is presented here in Fig. S5. The fast rise time from the revised fit is up to a few ps longer than the fast DB and VB anion decays at comparable excitation energies. Hence, the revised fitting of our previous data yields a more consistent set of time constants across the two systems and further supports the association of the fast decay constants for the TNIs with internal conversion (IC) to the ground state, followed by fragmentation to I^- .

In $I^- \cdot \text{CH}_3\text{NO}_2$ clusters photoexcited near their VDE, the DB to VB anion transition is complete and occurs within 500 fs. In those species, a long, clearly mono-exponential I^- re-formation rise time was observed to be an order of magnitude

slower than the fast component of the VB anion bi-exponential decay (21 ps vs 2 ps, respectively).⁴⁶ This delay was attributed to a dynamical bottleneck between IC and photofragmentation to I^- . For both $I^- \cdot U$ and $I^- \cdot U \cdot H_2O$, in which the DB anion does not undergo a complete VB conversion, it is possible that IC of the DB anion leads to the fast I^- rise component observed here for both systems, while the slow I^- rise is from internal conversion of the VB anion and significantly delayed iodide ejection, as in $I^- \cdot CH_3NO_2$.

For $I^- \cdot U \cdot H_2O$, we must also consider that the production of $I^- \cdot H_2O$ may also be an active decay channel here following internal conversion, as the asymptotic barrier to dissociation of water from uracil was calculated here to be less than 0.5 eV (1); however, the binding energy of this species (VDE = 3.51 ± 0.02 eV)^{47,48} is too high to photodetach in the present experiment. Once formed, $I^- \cdot H_2O$ could then dissociate on a longer time scale to yield I^- . Further experiments with a probe energy greater than 3.51 eV are planned to determine if $I^- \cdot H_2O$ formation is also a dissociation channel and measure the relevant time scales, as compared to the TNIs and iodide re-formation. It is also worth noting that I^- re-formation from $I^- \cdot U$ was measured with only one pump excitation energy at -80 meV, so the role of excitation energy dependence in directly comparing the $I^- \cdot U$ results with $I^- \cdot U \cdot H_2O$ is unclear.

The long-time decay of both the $I^- \cdot U \cdot H_2O$ DB anion and VB anion is likely to be autodetachment. Though difficult to record temporally, the photoelectron signal is measured here for 0 eV eKE electrons arising from autodetachment and has been measured previously for $I^- \cdot U$, among other systems.^{10,36,37} Here, the long-time decay of the $I^- \cdot U \cdot H_2O$ DB anion is quite similar to that of the +30 meV photoexcited $I^- \cdot U$ DB anion, consistent with the other lifetimes, as described above. The long decay time constant of the $I^- \cdot U \cdot H_2O$ VB anion, however, is quite a bit longer than that of the +30 meV photoexcited $I^- \cdot U$ VB anion, which could arise from the presence of water stabilizing the VB anion relative to autodetachment. Theoretical work by Takayanagi *et al.* and Adamowicz *et al.* on $U^- \cdot H_2O$ clusters predicts the VB anion to be stabilized more than the DB anion due to the increased excess electron density on the uracil ring for the VB anion compared to the diffuse DB anion.^{21,23,24} Although here the DB anion to VB anion conversion is not found to be faster nor have a smaller population intensity ratio of the DB anion to VB anion (Table III), this very long VB anion lifetime may indicate that the VB anion is preferentially stabilized to autodetachment.

As indicated earlier, the water molecule is known to be associated with both of the TNIs due to the increased eBEs of the features, but neutral iodine may leave the $I^- \cdot U \cdot H_2O$ DB anion in approximately 15 ps, as evidenced in the VDE shifting dynamics (Fig. 4). It is possible that neutral iodine loss similarly occurs for the VB anion, which for both species would leave behind a $U^- \cdot H_2O$ anion capable of decay only by autodetachment rather than internal conversion. Interestingly, a recent study of photofragment action spectroscopy of photoexcited $I^- \cdot U$ clusters found that electron detachment dissociation channels, rather than ionic photofragment formation channels, were the dominant decay pathways for the non-hydrated clusters, and these electron

detachment pathways are expected to be important here as well, as exemplified by the relatively large A_3 exponential amplitude for the $I^- \cdot U \cdot H_2O$ VB anion long decay (Table III).⁴⁹

VI. CONCLUSIONS

$I^- \cdot U \cdot H_2O$ clusters have been investigated using TRPEI to examine the dynamics of low energy electron attachment to uracil-water following the photoexcitation of the clusters near the cluster VDE of 4.40 eV, where a DB state of the overall complex is accessed. We observe the formation of the DB and VB TNIs of $I^- \cdot U \cdot H_2O$ and the relative stabilization of these anions in the presence of water, as indicated by an increase in the binding energy of both TNIs. The DB anion for $I^- \cdot U \cdot H_2O$ appears promptly, whereas there is a ~ 400 fs delay in the appearance of the VB anion. This delay, which is more pronounced than in $I^- \cdot U$,¹⁰ is attributed to a partial conversion of the DB to VB anion. The DB anion also exhibits a monotonically increasing VDE shift over 15 ps, reflecting stabilization of the DB state followed by the loss of a neutral I atom.

The TNIs exhibit bi-exponential decay, and the I^- photofragment signals exhibit a bi-exponential rise with time constants of 6.7 ps and 320 ps. Comparison of these time constants, along with those seen previously for $I^- \cdot U$ ^{10,13} and $I^- \cdot CH_3NO_2$,^{45,46} suggests that fast decay of the TNIs reflects internal conversion to the anion ground state in which the electron has back-transferred to the I atom, followed by fragmentation to I^- . We speculate that the fast and slow components of the I^- rise reflect IC from the DB and VB anions, respectively. At longer times, the TNIs likely decay by autodetachment, with the VB anion exhibiting a long decay time which suggests that it is stabilized relative to autodetachment by the presence of water.

SUPPLEMENTARY MATERIAL

See [supplementary material](#) for the following additional six figures: a waterfall plot view of the TRPEI data presented here in Fig. 2, a zoomed view of features C (autodetachment) and D (photodetachment of I^-) in the TRPEI data presented here in Fig. 3, a waterfall plot view of the TRPEI data presented here in Fig. 3 with feature C omitted, EOM-CCSD calculated images of the DB orbital as well as the π^* orbital for $I^- \cdot U \cdot H_2O$, a comparison of a mono-exponential rise fit to a bi-exponential rise fit for the I^- photofragment feature from Li *et al.*, Ref. 13, and the normalized integrated intensities for features E and E'. Possible assignments for the identities of features E and E' are also explored in the [supplementary material](#). An additional table is also provided to display the structures and dipole moments for neutral iodine-uracil-water and neutral uracil-water.

ACKNOWLEDGMENTS

This research was funded by the National Science Foundation under Grant No. CHE-1663832. A.K. acknowledges Government support awarded by DoD, Air Force Office of

Scientific Research, National Defense Science, and Engineering Graduate (NDSEG) Fellowship, 32 CFR 168a.

- ¹B. Boudaïffa, P. Cloutier, D. Hunting, M. A. Huels, and L. Sanche, *Science* **287**(5458), 1658–1660 (2000).
- ²R. Barrios, P. Skurski, and J. Simons, *J. Phys. Chem. B* **106**, 7991 (2002).
- ³J. Simons, *Acc. Chem. Res.* **39**, 772 (2006).
- ⁴H.-Y. Chen, P.-Y. Yang, H.-F. Chen, C.-L. Kao, and L.-W. Liao, *J. Phys. Chem. B* **118**, 11137 (2014).
- ⁵R. A. Bachorz, W. Klopper, M. Gutowski, X. Li, and K. H. Bowen, *J. Chem. Phys.* **129**, 054309 (2008).
- ⁶C. Desfrancois, H. Abdoul-Carime, and J.-P. Schermann, *Int. J. Mod. Phys. B* **10**, 1339 (1996).
- ⁷P. D. Burrow, G. A. Gallup, A. M. Scheer, S. Denifl, S. Ptasinska, T. D. Märk, and P. Scheier, *J. Chem. Phys.* **124**, 124310 (2006).
- ⁸G. Hanel, B. Gstir, S. Denifl, P. Scheier, M. Probst, B. Farizon, M. Farizon, E. Illenberger, and T. D. Märk, *Phys. Rev. Lett.* **90**, 188104 (2003).
- ⁹S. Ptasinska, S. Denifl, S. Gohlke, P. Scheier, E. Illenberger, and T. D. Märk, *Angew. Chem., Int. Ed.* **45**, 1893 (2006).
- ¹⁰S. B. King, M. A. Yandell, A. B. Stephansen, and D. M. Neumark, *J. Chem. Phys.* **141**, 224310 (2014).
- ¹¹S. B. King, A. B. Stephansen, Y. Yokoi, M. A. Yandell, A. Kunin, T. Takayanagi, and D. M. Neumark, *J. Chem. Phys.* **143**, 024312 (2015).
- ¹²A. B. Stephansen, S. B. King, Y. Yokoi, Y. Minoshima, W.-L. Li, A. Kunin, T. Takayanagi, and D. M. Neumark, *J. Chem. Phys.* **143**, 104308 (2015).
- ¹³W.-L. Li, A. Kunin, E. Matthews, N. Yoshikawa, C. E. H. Dessent, and D. M. Neumark, *J. Chem. Phys.* **145**, 044319 (2016).
- ¹⁴J. Schiedt, R. Weinkauff, D. M. Neumark, and E. W. Schlag, *Chem. Phys.* **239**, 511 (1998).
- ¹⁵K. Khistyayev, A. Golan, K. B. Bravaya, N. Orms, A. I. Krylov, and M. Ahmed, *J. Phys. Chem. A* **117**, 6789 (2013).
- ¹⁶Y. He, C. Wu, and W. Kong, *J. Phys. Chem. A* **107**, 5145 (2003).
- ¹⁷Y. He, C. Wu, and W. Kong, *J. Phys. Chem. A* **108**, 943 (2004).
- ¹⁸J. H. Hendricks, S. A. Lyapustina, H. L. de Clercq, J. T. Snodgrass, and K. H. Bowen, *J. Chem. Phys.* **104**, 7788 (1996).
- ¹⁹R. N. Compton, H. S. Carman, C. Desfrancois, H. Abdoulcarime, J. P. Schermann, J. H. Hendricks, S. A. Lyapustina, and K. H. Bowen, *J. Chem. Phys.* **105**, 3472 (1996).
- ²⁰O. Dolgounitcheva, V. G. Zakrzewski, and J. V. Ortiz, *J. Phys. Chem. A* **103**, 7912 (1999).
- ²¹J. H. Hendricks, S. A. Lyapustina, H. L. de Clercq, and K. H. Bowen, *J. Chem. Phys.* **108**, 8 (1998).
- ²²N. A. Oyler and L. Adamowicz, *J. Phys. Chem.* **97**, 11122 (1993).
- ²³C. A. Morgado, K. Y. Pichugin, and L. Adamowicz, *Phys. Chem. Chem. Phys.* **6**, 2758 (2004).
- ²⁴H. Motegi and T. Takayanagi, *J. Mol. Struct.: THEOCHEM* **907**, 85 (2009).
- ²⁵T. Frigato, D. Svozil, and P. Jungwirth, *J. Phys. Chem. A* **110**, 2916 (2006).
- ²⁶Calculated in the present study using the Gaussian 09 computing package at the MP2/aug-cc-pVDZ(-pp) level of theory; see Methods section for computational details.
- ²⁷R. J. Peláez, C. Blondel, C. Delsart, and C. Drag, *J. Phys. B: At., Mol. Opt. Phys.* **42**, 125001 (2009).
- ²⁸A. V. Davis, R. Wester, A. E. Bragg, and D. M. Neumark, *J. Chem. Phys.* **118**, 999 (2003).
- ²⁹A. E. Bragg, J. R. R. Verlet, A. Kammrath, O. Cheshnovsky, and D. M. Neumark, *J. Am. Chem. Soc.* **127**, 15283 (2005).
- ³⁰W. C. Wiley and I. H. McLaren, *Rev. Sci. Instrum.* **26**, 1150 (1955).
- ³¹A. Eppink and D. H. Parker, *Rev. Sci. Instrum.* **68**, 3477 (1997).
- ³²V. Dribinski, A. Ossadtchi, V. Mandelshtam, and H. Reisler, *Rev. Sci. Instrum.* **73**, 2634 (2002).
- ³³M. J. Frisch, G. W. Trucks, H. B. Schlegel, G. E. Scuseria, M. A. Robb, J. R. Cheeseman, G. Scalmani, V. Barone, B. Mennucci, G. A. Petersson, H. Nakatsuji, M. Caricato, X. Li, H. P. Hratchian, A. F. Izmaylov, J. Bloino, G. Zheng, J. L. Sonnenberg, M. Hada, M. Ehara, K. Toyota, R. Fukuda, J. Hasegawa, M. Ishida, T. Nakajima, Y. Honda, O. Kitao, H. Nakai, T. Vreven, J. A. Montgomery, Jr., J. E. Peralta, F. Ogliaro, M. J. Bearpark, J. Heyd, E. N. Brothers, K. N. Kudin, V. N. Staroverov, R. Kobayashi, J. Normand, K. Raghavachari, A. P. Rendell, J. C. Burant, S. S. Iyengar, J. Tomasi, M. Cossi, N. Rega, N. J. Millam, M. Klene, J. E. Knox, J. B. Cross, V. Bakken, C. Adamo, J. Jaramillo, R. Gomperts, R. E. Stratmann, O. Yazyev, A. J. Austin, R. Cammi, C. Pomelli, J. W. Ochterski, R. L. Martin, K. Morokuma, V. G. Zakrzewski, G. A. Voth, P. Salvador, J. J. Dannenberg, S. Dapprich, A. D. Daniels, Ö. Farkas, J. B. Foresman, J. V. Ortiz, J. Cioslowski, and D. J. Fox, GAUSSIAN 09, Revision C.01, Gaussian, Inc., Wallingford, CT, USA, 2009.
- ³⁴K. A. Peterson, B. C. Shepler, D. Figgen, and H. Stoll, *J. Phys. Chem. A* **110**, 13887 (2006).
- ³⁵J. E. Sansonetti and W. C. Martin, *J. Phys. Chem. Ref. Data* **34**, 1559 (2005).
- ³⁶M. A. Yandell, S. B. King, and D. M. Neumark, *J. Am. Chem. Soc.* **135**, 2128 (2013).
- ³⁷S. B. King, M. A. Yandell, and D. M. Neumark, *Faraday Discuss.* **163**, 59 (2013).
- ³⁸J. Smets, W. J. McCarthy, and L. Adamowicz, *J. Phys. Chem.* **100**, 14655 (1996).
- ³⁹J. Smets, D. M. A. Smith, Y. Elkadi, and L. Adamowicz, *J. Phys. Chem. A* **101**, 9152 (1997).
- ⁴⁰T. van Mourik, S. L. Price, and D. C. Clary, *J. Phys. Chem. A* **103**, 1611 (1999).
- ⁴¹H.-Y. Chen and W.-S. Sheu, *J. Am. Chem. Soc.* **122**, 7534 (2000).
- ⁴²H.-Y. Chen and W.-S. Sheu, *Chem. Phys. Lett.* **335**, 475 (2001).
- ⁴³Q. K. Timerghazin and G. H. Peslherbe, *J. Am. Chem. Soc.* **125**, 9904 (2003).
- ⁴⁴F. D. Vila and K. D. Jordan, *J. Phys. Chem. A* **106**, 1391 (2002).
- ⁴⁵M. A. Yandell, S. B. King, and D. M. Neumark, *J. Chem. Phys.* **140**, 184317 (2014).
- ⁴⁶A. Kunin, W.-L. Li, and D. M. Neumark, *Phys. Chem. Chem. Phys.* **18**, 33226 (2016).
- ⁴⁷G. Markovich, R. Giniger, M. Levin, and O. Cheshnovsky, *J. Chem. Phys.* **95**, 9416 (1991).
- ⁴⁸G. Markovich, S. Pollack, R. Giniger, and O. Cheshnovsky, *J. Chem. Phys.* **101**, 9344 (1994).
- ⁴⁹E. Matthews, R. Cercola, G. Mensa-Bonsu, D. M. Neumark, and C. E. H. Dessent, *J. Chem. Phys.* **148**, 084304 (2018).